Lab on a Chip

RSC Publishing

PAPER

View Article Online
View Journal | View Issue

Microfluidic chemostat for measuring single cell dynamics in bacteria†

Cite this: *Lab Chip*, 2013, **13**, 947

Zhicheng Long,[a] Eileen Nugent,[b] Avelino Javer,[b] Pietro Cicuta,[b] Bianca Sclavi,[c] Marco Cosentino Lagomarsino[def] and Kevin D. Dorfman*[a]

Received 27th October 2012,
Accepted 21st December 2012

DOI: 10.1039/c2lc41196b

www.rsc.org/loc

We designed a microfluidic chemostat consisting of 600 sub-micron trapping/growth channels connected to two feeding channels. The microchemostat traps *E. coli* cells and forces them to grow in lines for over 50 generations. Excess cells, including the mother cells captured at the start of the process, are removed from both ends of the growth channels by the media flow. With the aid of time-lapse microscopy, we have monitored dynamic properties such as growth rate and GFP expression at the single-cell level for many generations while maintaining a population of bacteria of similar age. We also use the microchemostat to show how the population responds to dynamic changes in the environment. Since more than 100 individual bacterial cells are aligned and immobilized in a single field of view, the microchemostat is an ideal platform for high-throughput intracellular measurements. We demonstrate this capability by tracking with sub-diffraction resolution the movements of fluorescently tagged loci in more than one thousand cells on a single device. The device yields results comparable to conventional agar microscopy experiments with substantial increases in throughput and ease of analysis.

Introduction

Microfluidic devices have become an attractive platform for cell biology over the past decade.[1–5] With the help of advanced microfabrication technologies, researchers have developed numerous microdevices and protocols to trap, manipulate, grow and analyze different types of cells.[6–8] Many of these devices were designed to handle large, immobile eukaryotic cells with diameters ranging from several microns to tens of microns. Developing similar protocols for small, motile prokaryotic cells such as bacteria is considerably more challenging, especially when one accounts for the fast cell division rate.

One possible approach to study bacteria at the single-cell level is to confine the bacteria in individual chambers, with one bacterium per chamber. For example, Groisman *et al.* built a PDMS chemostat device containing an array of fluidic channels and shallow chambers.[9] In this device, a single bacterial cell, loaded into the chamber, develops into a colony. Droplet confinement is an alternate approach to confine the bacteria. Using this approach, Boedicker *et al.* studied the quorum sensing behavior and the growth of single bacterial cells by confining them into small droplets of 100 fL in volume.[10] Park *et al.* also demonstrated co-cultivation of microbial communities in parallel aqueous droplets dispersed in a continuous oil phase.[11]

The main advantage of isolation methods, either in chambers or droplets, is the ability to study single cells in the absence of communication, or to study communication such as quorum sensing in a controlled environment with only a few cells. However, the observation time in either microchambers or droplets is limited to several generations because bacterial cells grow and divide so quickly that the cells quickly overwhelm the small space and exhaust nutrients in a few hours. Indeed, one experiences similar issues in traditional agar-based experiments, as the nutrients are depleted and the colony eventually buckles due to the stress of continuous outward expansion. If one wishes to make long-time measurements of dividing cells at the single-cell level, it is essential that (i) the nutrient supply be continuously replenished and (ii) excess bacterial cells escape out of the trap to maintain a quasi-steady state population density.

Several competing approaches to implement long-time measurements have appeared in the literature. The first approach uses ~1-μm-deep flat chambers with one or two sides open to media channels in a PDMS device.[12] This device allows a two-dimensional colony of *E. coli* to grow over many generations; the colony is fed by the flow along the open sides

[a]*Department of Chemical Engineering and Materials Science, University of Minnesota - Twin Cities, 421 Washington Ave. SE, Minneapolis, MN 55455, USA. E-mail: dorfman@umn.edu*
[b]*Cavendish Laboratory, University of Cambridge, Cambridge CB3 0H3, UK*
[c]*LBPA, UMR 8113 du CNRS, École Normale Supérieure de Cachan, France*
[d]*University Pierre et Marie Curie, 15 rue de l'École de Médecine, Paris, France*
[e]*CNRS, UMR 7238 'Microorganism Genomics', Genomic Physics Group, 15 rue de l'École de Médecine, Paris, France*
[f]*University of Turin, Physics Department, Via P. Giuria 1-10125 Torino, Italy*
† Electronic supplementary information (ESI) available: Supplementary movies. See DOI: 10.1039/c2lc41196b

of the chamber and cells at the edge of the colony are continuously swept away by the aforementioned flow. Similarly, Grünberger *et al.* fabricated picolitre volume bioreactors with a 1-μm-deep culturing region, which forces the bacterial cells to grow into monolayer microcolonies of up to 500 cells and allows the excess cells to escape from the overflow channels.[13] While these devices are quite simple to fabricate, the cells in the colony are randomly packed inside the chamber. As a result, the image analysis in the device is as difficult as analyzing a colony on agar. Moreover, the cells at the center of the colony rarely reach the edges of the trapping region. As a result, different cells in the colony have different ages, the cellular lineages are challenging to identify, and the accumulation of mutations may become an issue during long-time measurements. It is also unclear whether one-dimensional confinement is sufficient to provide the immobilization required for tracking sub-cellular fluorescently labeled proteins. For example, the loci tracking experiments we present here involve total displacements on the order of 100 nm.[14] If the cells are able to move laterally, it will be impossible to decouple the random motion of the cell from the random motion of the locus.

The second approach grows *E. coli* cells in an array of 2000(L) × 3(W) × 1(D)-μm micro-grooves fabricated on a glass coverslip.[15] The grooves are covered by a streptavidin-decorated semi-permeable membrane that allows nutrient exchange by diffusion. The cells coming out of the membrane-covered region are washed away by the medium flow. The fluid transport in this device also allows for good transport of nutrients. Wakamoto *et al.* used such device to study age distributions along lineages within populations of bacterial cells.[15] Compared with above flat chamber method, the 3-μm-wide growth channels simplify the image analysis to some extent but still do not provide any cell orientation. The minimal confinement in this device does not permit sub-diffraction imaging.

The image processing and lineage issues are simplified in the third approach, known as the ''mother machine''.[16] Here, a series of short, dead-ended growth channels extend from a central feeding channel. The original cell entering a given dead-end channel is the ''mother'' cell, and all subsequent cells in a given channel result from cell division from the mother. When a daughter cell reaches the end of the dead-end channel, it is removed by the nutrient flow. In this manner, Wang *et al.* forced bacterial cells to grow one-dimensionally at steady growth rate for more than 100 generations.[16] This device is an excellent platform to study aging of bacteria, since the original mother cell is trapped at the dead-end, and an improvement over the flat chamber method[12,13] because the cell lineage is easily identified. However, the device is less attractive if one wants to obtain single-cell data while controlling for the age effects, since the accumulation of mutations and non-genetic effects leads to changes in the population with time (*e.g.*, filamentation[16]). Moreover, as was the case in the devices discussed so far, the bacteria are not strongly immobilized in this device. While the mother machine allows one to obtain data on growth rates and overall fluorescence, tracking small fluorescent reporters with nanometer resolution is not possible.

More recently, Moffitt *et al.* described a fourth approach by molding agarose to create linear tracks, separated by gutters.[17] This single-cell chemostat also forces bacterial cells to grow linearly in the small tracks and allows excess cells to escape from both ends. They grew various bacteria chemostatically on the device for over 30–40 generations, demonstrating that the device avoids the exponential growth problem in conventional agar devices. The cells still communicate through the highly porous agarose walls, maintaining colony-like behavior and the ability to co-culture different cell types inside the device. This agarose-based microdevice has some advantages over those made with PDMS, in particular using a ubiquitous material in conventional microbiology experiments. However, the high porosity of agarose makes it difficult to change the growth media inside, which limits its use to applications that do not require media change. When the media inside the gutters is replaced by changing the composition of the single inlet to this device, diffusion can quickly replace the media inside the tracks. However, nutrients in the saturated agarose will be leached by diffusion into the tracks for long times. To estimate this time scale, we note that the agarose pad in this device is roughly 1 cm thick and the typical diffusion coefficient in agarose for small molecules, such as glucose,[18] is 10^{-5} cm^2 s^{-1} and decreases to 10^{-7} cm^2 s^{-1} for larger molecules, such as bovine serum albumin (BSA).[19] Even if the entire agarose pad is not saturated, the corresponding diffusion time is still hours. As a result, the porosity of the agarose is also undesirable for experiments where one wants to study the dynamics of single cells in isolation or to have a rapid exchange of the media.

In this work, we describe a PDMS-based microfluidic chemostat that we believe combines the best features of the aforementioned devices for interrogating isolated, single cells while avoiding their shortcomings in media exchange or bacteria immobilization. Explicitly, our device allows for (i) continuous, dynamic control over the flow of nutrients, (ii) minimal communication between cells in the device, (iii) control over the number and orientation of the cells, (iv) a population of cells which is homogeneous in terms of age and (v) sufficient immobilization to permit sub-diffraction imaging and tracking of fluorescently labeled loci. The open-end channel design in our device leads to fast loading of bacterial cells into the growth channel. It also allows us to maintain a weak flow in the growth channels to provide steady nutrient source for the growing bacterial cells. By carefully controlling the channel geometry, we could keep the bacteria growing chemostatically for several days in a persistent young state. We could thus monitor the growth dynamics at the single cell level for long times by time-lapse microscopy, while also retaining the ability to change the growth media during the measurement. We can also perform intracellular measurements on thousands of aligned individual bacterial cells on a single device. Our device does not appear to exhibit any of the

potential bio-shortcomings of aligning bacteria in a PDMS-based device for long-term culture,[17] opening the way for continued advances in PDMS technologies in this area.

Experimental section

Microchemostat design and fabrication

As shown in Fig. 1, the microchemostat resembles a ladder. We fabricated 600 narrow and shallow channels on a PDMS device to trap the *E. coli* cells. These trapping/growth channels (rungs) are about 20 μm long, 0.6 to 0.9 μm wide and 1.1 μm deep. The rungs are connected to a pair of 50 μm wide and approximately 20 μm deep feeding channels. The media flow in the feeding channels continuously delivers fresh nutrients to the bacterial cells inside the rungs and washes away the excess cells.

Fabrication of the silicon master for preparing the PDMS replica started with the patterning of the small rungs using Shipley 1813 positive photoresist. Due to the resolution limitation (1.3 μm) of the mask-making equipment, we performed an oxygen plasma thinning process[20] to shrink the width of the resist pattern of the rungs, allowing us to use a single mask while tuning the size of the trapping channels to fit the cell size at different growth conditions. The bulk silicon was then etched down to ~1.1 μm in a reactive ion etcher to obtain the positive reliefs of the rungs. After cleaning the wafer and inspecting the rungs by optical microscopy and profilometry, the positive reliefs of the larger feeding channels were photolithographically patterned in SU-8 negative photoresist.

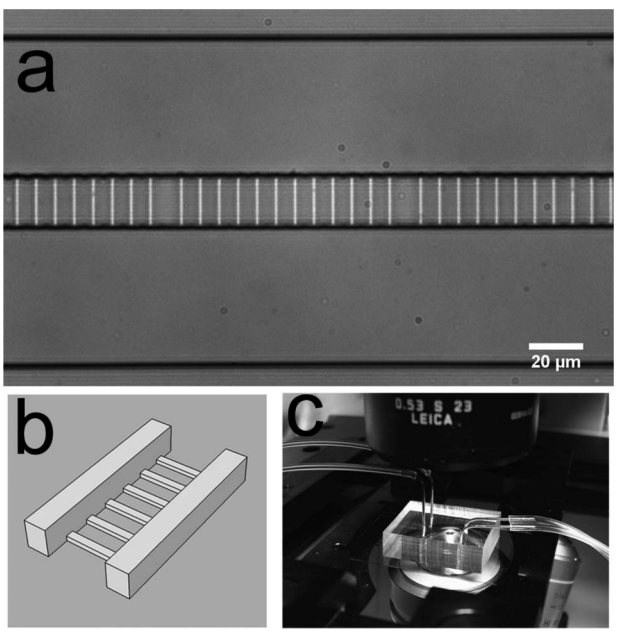

Fig. 1 The microfluidic chemostat. (a) Micrograph of the trapping/growth channels (center) connected to two large feeding channels. The occasional gaps between trapping channels are used as counters for the channel number. (b) Schematic illustration of ladder-like microchemostat. (c) The PDMS device connected to inlet-outlet tubes on the microscope stage.

Before casting the PDMS prepolymer, the silicon master was first silanized in a vapor of (Tridecafluoro-1,1,2,2,-tetrahydrooctyl)trichlorosilane for approximately 30 min. A 10 : 1 w/w mixture of PDMS base and curing agent (Sylgard 184, Ellsworth Adhesives) was then poured over the master and cured in an oven at 75 °C for at least 6 h. The cured PDMS stamp was peeled from the silicon master and cut into individual chips. After inlet-outlet holes were cut with a Harris Uni-Core 0.75 mm punch (Ted pella, Inc.), the PDMS chips were irreversibly sealed with clean glass coverslips by treating them in air plasma (Harrick Plasma).

Loading and growing *E. coli* cells in the microchemostat

Two syringe pumps (Harvard 11 Plus) were used to drive the solutions into the PDMS feeding channels. In order to prevent cell adhesion to the PDMS surface, all of the channel walls were passivated by flowing a 20 mg mL^{-1} BSA solution for at least one hour. Following the passivation step, both pumps were filled with culture medium and a plug of fresh, log-phase *E. coli* suspension was aspirated into one of the inlet tubes.

We developed a two-step procedure for loading the bacterial cells into the small trapping channels. We began with a relatively high flow rate; the volumetric flow rate (>5 μL min^{-1}) in the loading channel, which is pumping the bacteria into the device, is much greater than the volumetric flow rate (0.4 μL min^{-1}) in the balancing channel. The concomitant difference in pressure across the rungs of the ladder leads to a relatively strong flow across each rung. The pressure may also deform the elastomeric PDMS walls, which allows the bacteria to more easily flow through the rungs. Once we observed that most of the rungs had bacteria flowing through them, we reduced the flow rates to 0.4 μL min^{-1} and 0.2 μL min^{-1}, respectively. The bacteria then became trapped inside the rungs.

When the bacteria are trapped, the hydrodynamic resistance of the rungs increases and there is only a weak flow through the rungs. This flow is sufficient to provide a steady source of nutrients but does not perturb the locations of the bacteria. When we maintain the low flow rates in both feeding channels, the bacteria keep growing and dividing in lines inside the growth channels and the excess cells are pushed out into the feeding channels and washed away by the flow.

Bacterial strains and growth conditions

Escherichia coli K-12 strain BW25113 carrying the PKK_PdnaA_GFP plasmid[21] was used for the growth experiments. The strain used for expression experiments contains a chromosomal P*gyrA*-GFP reporter gene construct, where the expression of the GFP is under control of the P*gyrA* promoter, inserted between the yggG and tktA genes on the Mc-Gal1 strain (MC4100 derivative). The strains used for loci tracking were derivatives of *E. coli* MG 1655 or MG 1657 with P1parS inserted at 9 different positions around the chromosome. The expression of the ParB-GFP fusion protein is driven by the pALA2705 plasmid.[22]

Strains were first grown overnight in Luria Broth (LB) medium at 37 °C with either ampicillin at 100 μg mL^{-1} or kanamycin at 50 μg mL^{-1}. The cultures were then diluted 1000 fold in liquid M9 minimal media (12.8 g L^{-1} $Na_2HPO_4 \cdot 7H_2O$; 3 g L^{-1} KH_2PO_4; 1 g L^{-1} NH_4Cl; 0.5 g L^{-1} NaCl; 0.1 mM $CaCl_2$; 2 mM $MgSO_4$; 0.02 mg ml^{-1} Tryptophan; 0.025 mg ml^{-1}

Thymidine) supplemented with 0.4% glucose or 0.4% glucose and 0.5% casamino acids. The growth media included appropriate antibiotics, which are indicated in the relevant points in the text. Cultures were grown at 37 °C to mid-log phase. After being loaded into the microchemostat, the *E. coli* cells continued growing in the trapping channels in the same or different M9 media, as indicated in the relevant figures.

Time-lapse microscopy

Time-lapse movies were recorded on a fully automated inverted microscope (Leica DMI-4000B) equipped with a motorized stage (Prior Scientific) and an external Leica EL6000 light source for fluorescence. A Photometrics CoolSnap EZ CCD camera was used to collect the images. The microscope and the stage were controlled with the open-source Micro-manager software.[23] Autofocus was achieved through the embedded JAF (H&P) autofocus module and was performed at every time point on the phase contrast channel. The growth experiments and the loci tracking experiments at Minnesota were carried out at room temperature (~25 °C), while expression experiments for the reporter gene were performed at 30 °C by placing the PDMS device in a custom made, heated aluminum holder.

Typically, twelve growth channels were observed in the field of view of an oil-immersion 100× phase contrast objective with numerical aperture of 1.3. The microscope automatically moves through different fields of view to obtain data across the entire device at different time points. For single-cell GFP expression experiments, images on phase contrast and fluorescence were collected from four fields of view at intervals of 2 min and 10 min, respectively. For loci tracking experiments, we first kept the cells growing for 6 h while phase contrast images were captured every minute to calculate the growth rate. We then recorded the movement of fluorescently tagged loci in burst mode with 100 ms exposure for 15 to 20 fields of view.

Additional growth experiments in the chip, used for Fig. 2a, were performed in Cambridge on a Nikon TI eclipse inverted microscope using a Nikon intensilight light source for fluorescence. Images were collected on an Andor iXon EMCCD camera. Cells were imaged through a 63× oil immersion objective with a numerical aperture of 1.4. Stage and microscope control was performed using customized automation routines written in C. Focus was maintained throughout the experiment with Nikon perfect-focus hardware focusing. Growth experiments were performed at 37 °C. Fluorescence images were collected every 2 mins from 15 fields of view with typically 7 channels in each field of view. We performed the latter experiments at 37 °C to demonstrate the ability of our apparatus to work at elevated temperatures as well as room temperature.

Image analysis

For the growth data in Fig. 2a images were segmented and tracked across frames using a custom program written in Matlab (Mathworks). All other cell segmentation and fluorescence measurements were performed with the open-source software 'Cellprofiler'.[24] We used the 'RobustBackground Adaptive' thresholding method in this software program to identify the boundaries of the fluorescent cells. The movements of loci were tracked and analyzed using a custom program written in Matlab. Only mean square displacements at time scale of 0.1 to 5 s were used for fitting analysis. Growth rates of the cells were calculated manually from the phase contrast or fluorescence movies.

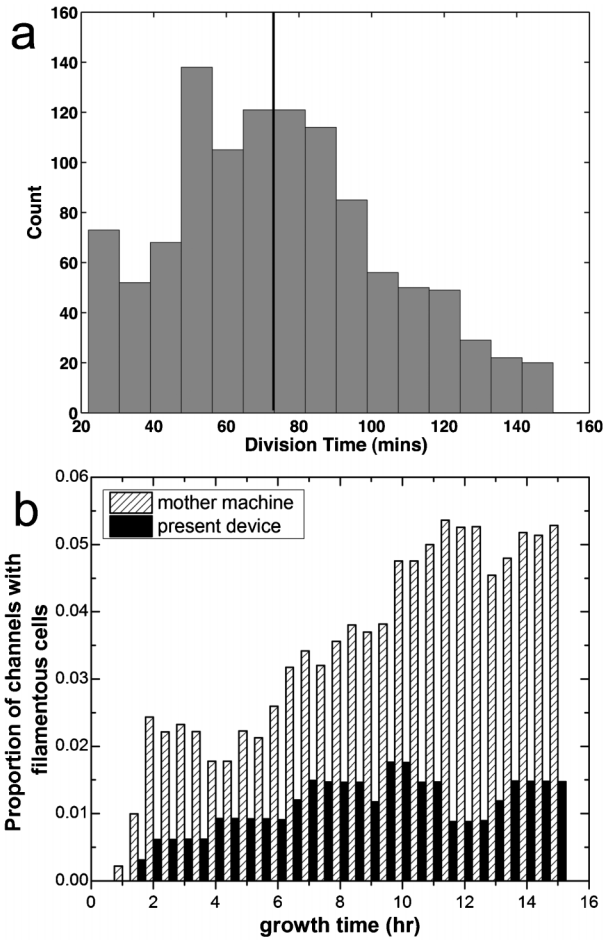

Fig. 2 (a) Distribution of division times of *E. coli* cells with a P*gyrA*-GFP reporter gene construct in the microchemostat. Cells were grown at 37 °C in M9 minimal medium supplemented with 0.4% glucose, 0.5% casamino acids and 0.1% BSA. The mean growth rate in the microchemostat is 75 mins. This is comparable to the bulk doubling time of 73 mins, which is indicated as a line on the above plot. Bulk growth was obtained from optical density measurements of cells cultured in 50 ml tubes. (b) Proportion of growth channels with filamentous cells among all occupied channels in the present open-channel device and a dead-end ''mother machine'' device[16] as a function of time. The fraction of occupied channels in both devices remains relatively stable after loading (mother machine, 92.5% to 81.4%, present microchemostat, 53.8% to 56.8%). *E. coli* strains BW25113 carrying the PKK_PdnaA_GFP plasmid were grown inside both devices at room temperature (~25 °C) in LB media with 100 μg mL^{-1} ampicillin. The mother machine contains 1000 dead-end, ~20(L) × 1.5(W) × 1.1(D)-μm growth channels. Flow rates in the feeding channel (50 μm wide and ~20 μm deep) of the mother machine were maintained at 20 μL min^{-1}.

Results and discussion

Bacterial growth in the microfluidic chemostat

Unlike the dead-end configuration of the ''mother machine'',[16] the growth channels in the present microfluidic chemostat are

connected to a pair of large feeding channels on both ends. This open-end design is more flexible and easier to operate than the ''mother machine''. First, the open-ended design permits faster loading of cells into the growth channels. In the experiments described here, the bacteria cells were loaded into the sub-micron channels by the pressure difference between the two feeding channels. The loading process typically took less than five minutes. In contrast, loading cells into a dead-end channel requires slow diffusion from a very dense cell suspension. In our experience, loading the mother machine takes several hours, while the open-ended design loads in a few minutes. Second, the open-end chemostat allows the old mother cells to exit the growing channel after cell elongation and division, which is especially useful when cells of similar age are desired. By contrast, the mean cell age increases over the experimental time in a dead-ended mother machine. Third, one can maintain a weak flow in the growth channels at relatively low flow rates (less than 1 μL min^{-1}) to provide steady nutrient source for the growing bacterial cells. One has to maintain flow rates in the feeding channel higher than 15 μL min^{-1} to ensure sufficient nutrients delivery to the dead-end growth channels. This is a potential issue, since higher flow rates often cause leaks in PDMS devices. Also, the open-end design allows for the quick change of the growth media in the growth channels during observation.

The use of open-ended, short growth channels certainly gives rise to the concern that the bacteria can escape from the trapping channels by swimming or by entrainment in the flow inside a rung. We thus investigated the effect of the trapping/growth channel dimensions on the long-term growth of *E. coli* in the device. We made a range of trapping channels of various widths, using the plasma thinning method,[20] and then etched their molds to a fixed depth of approximately 1.1 μm. We then loaded and grew GFP-expressing *E. coli* cells on these devices in M9 media supplemented with 0.4% glucose and 1% casamino acids and 50 μg mL^{-1} ampicillin. For devices with growth channel widths larger than 1.2 μm, the bacterial cells (~0.8 μm diameter for this particular media) flowed through the trapping channels easily and hardly stopped therein, even at slow flow rates. The cells could be easily trapped inside ~1.0 μm wide channels using the loading protocol described above. However, the number of cells in each channel decreased after growing for several hours, as seen in movie s1. When the width of the trapping channels is less than around 0.8 μm, roughly equal to the cell diameter, a loading flow rate larger than 10 μL min^{-1} was required to push the cells inside the rungs. Once the bacteria are trapped in such small channels, the cells are immobilized provided that the flow rate difference between the two feeding channels is lower than 2.0 μL min^{-1}. As a consequence, we could maintain a very high and stable cell population for as long as three days (see movie s2). Although Mannik *et al.* had reported that bacterial cells could grow and penetrate small channels of 0.4 μm wide by significant deformation,[25] it is very hard to load cells (~0.8 μm diameter) into channels narrower than 0.6 μm or shallower than 0.8 μm in our device. In any event, our goal is to observe large numbers of growing, isolated cells, so any mechanical strain that would occur when loading bacteria into nanochannels is undesirable.

Although the hydrodynamic resistance of the growth channels increases when they are filled with cells, a control experiment with fluorescent dye showed that there is flow across all of the bacteria filled channels at the working flow rates (movie s3). We think this flow is sufficient to provide a steady source of nutrients for the growing cells and removal of the waste created by cell growth.[26] In our experiments, the mean division time obtained from single cell measurements of *E. coli* cells growing in the rung channels (75 mins) is similar to the doubling time calculated from optical density measurements of bulk growth in 50 ml culture tubes (73 mins), as shown in Fig. 2a.

One of the key features of our device is the ability to maintain the cells at a relatively constant age. This provides an especially strong contrast with the dead-ended mother machine,[16] where the progenitor mother cell is trapped and the population inside the device gradually ages. To demonstrate the robustness of our device for aging control, we compared the increase in filamentation in the bacteria in our device to the filamentation in the mother machine while controlling for the bacteria strain and the growth conditions between the different devices. Filamentation is an important indicator of cell health. Wang *et al.*[16] previously reported that the filamentation rates of the mother cells trapped in the dead-end mother machine grow with replicative age and could be higher than 10% after 50 generations. Fig. 2b indicates that the proportion of the growth channels containing filamentous cells in the open-end device is much lower than that on the dead-end mother machine, using identical bacteria strain and growth conditions. Moreover, in a separate experiment, we observed that the filamentation rates in the present device did not increase with the growth time, even in the third day of growth. We attribute the low filamentation rate to the open-end channel design, which allows the old cells to exit the growth channels and thus allow us to maintain the cells at similar age.

Both the division time and the low filamentation rate observed in Fig. 2 imply that the growth of bacterial cells in the sub-micron channels was not perturbed by the confinement, as observed by other researchers.[16,17,25] Moreover, it allays fears about the properties of PDMS that motivated the development of agarose-based devices.[17] We also sometimes observe accumulation of bacteria near the inlets and outlets of the channel, usually in the third day of the experiment. These bacteria reduce the flow of nutrients into the rungs, which can slow down the growth rate in such an extremely long experiment.

Single-cell GFP expression

The microchemostat can continuously provide fresh media for the growing bacterial cells and remove the excess cells and waste from the growth channels resulting in constant, balanced growth. These features make it possible to study the bacterial growth dynamics at the single cell level for 40–50 generations while maintaining a steady, non-aging cell population at ~100 cells per field of view during the entire observation period. To demonstrate this capability, we constructed an *E. coli* strain containing the P*gyrA*-GFP reporter gene construct integrated on the chromosome, and then

monitored its growth dynamics and GFP expression in the microchemostat. Fig. 3 and movie s4 show the fluorescent cells growing in the sub-micron channels. This particular image also shows several cells exiting the ends of the rungs.

Our microchemostat design also permits facile changing of the growth medium. To demonstrate this second capability, we used a PDMS-based Y-shape mixer to change the growth media in both feeding channels without interrupting the image acquisition. In the experiment in Fig. 3, the cells first grew in a "slow" M9 media (with 0.4% glucose (Glu), ~160 mins doubling time) for around 13 h, then in a "fast" M9 media (with 0.4% glucose and 1% casamino acids (CAA), ~90 mins doubling time) for 11 h and again in the slow M9 media for another 12 h. During these experiments, phase contrast and fluorescence images were collected at intervals of 2 min and 10 min, respectively. The mean pixel intensity of the fluorescent cells in each frame were measured with Cellprofiler and plotted *versus* the growth time, as shown in Fig. 3b. The average GFP intensity drops quickly in the first two hours due to photobleaching and then reaches a stable value until the growth medium is changed. The fluorescence rises quickly (in ~2 h) when the growth medium was changed from slow M9 media (M9 + Glu) to faster M9 media (M9 + Glu + CAA). There is also an obvious overshoot before the fluorescence reaches the high stable level. There are also fluctuations in the intensity level even at the steady state. While these fluctuations could be due to the population heterogeneity, our experience with the experimental apparatus leads us to suspect that the dominant contributions are (i) the software-controlled autofocusing, which can lead to some defocusing during the experiment, and (ii) the slightly smaller size of the cells in the slow growth medium, which allows the cells to tilt in the vertical direction.

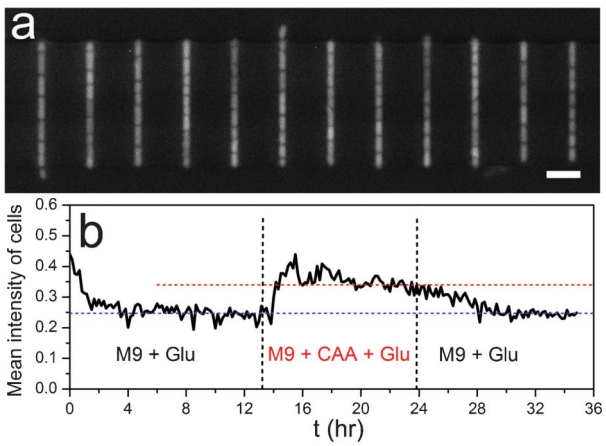

Fig. 3 Growth of *E. coli* cells with P*gyrA*-GFP reporter gene construct in the microchemostat. (a) Fluorescence image of the *E. coli* cells growing in the sub-micron channels. The cell at the top of the 6th rung is escaping into the feeding channel. The scale bar corresponds to 5μm. (b) The average GFP intensity of *E. coli* cells as a function of time. The experiment begins with M9 media supplemented with 0.4% glucose (Glu), switches to M9 with 0.4% glucose and 1% casamino acids (CAA), and then returns to the original medium. Both media contained 50 μg mL^{-1} kanamycin. Growth temperature was maintained constant at 30 °C.

The increase of fluorescence upon change in the growth medium can be explained by both the position of the GFP gene in the chromosome and the intrinsic growth rate dependence of the *PgyrA* promoter. The *PgyrA*-GFP construct in these experiments is at a site on the chromosome that is near the origin of DNA replication. At faster growth rates, *E. coli* cells will have on average more copies of the DNA that are near the origin. In this case, for example, one would expect about a 50% increase in gene copy number, which could thus suffice to explain the increase in fluorescence observed in our experiment. In addition, previous work by us and others has observed an increase in the activity of the *gyrA* promoter at faster growth rates,[27] however in these cases the *PgyrA* promoter was either found on a plasmid or at its original chromosomal site, near the terminus region. The overshoot could thus result from the increase in promoter activity.

When the growth medium is changed back to slow M9 media, the fluorescence decreases and eventually reaches the same stable level as in the first growth period. However, the decrease of the fluorescence in the downshift is slower (around 4 h) than the increase of fluorescence in the upshift, which implies that the adaptation of bacterial cells from nutrient-limited media to rich media is faster than that in reverse. The different adaptation time might be attributed to the difference of the protein dilution rate in growing cells, which is equal to the growth rate of the cell.[28]

Movement tracking of chromosomal loci

The bacterial chromosomal DNA is organized into a compact structure called the nucleoid. It is widely believed that the nucleoid's physical organization plays a major role in cell division, gene expression and other important cellular processes.[29] Tracking studies of fluorescently tagged chromosomal loci probe the local viscoelastic properties of the nucleoid and thus its physical organization, if the time scales are short (<1 min) compared to its segregation dynamics at longer time scales.[29] We think our microchemostat is an ideal platform for loci tracking because it allows one to image thousands of aligned bacterial cells at a time while maintaining all of the cells in similar age in identical and constant nutrient environments. By carefully controlling the size of the growth channels, we could load and grow bacterial cells in channels slightly narrower than the cell diameter. As a result, the cell movement inside the growth channels is minimized. The cells in other reported PDMS devices, such as the mother machine[16] and the shallow chambers,[12,13] are localized but not necessarily immobilized. Since the loci tracking requires tracking the fluorescent loci with a precision well below the diffraction limit, bacteria immobilization is critical.

To demonstrate this capability, we used nine strains containing P1parS inserted at various positions along the chromosome.[22] We grew these strains on the microchemostat in two different media: M9 media with 0.4% glucose or M9 media with 0.4% glucose and 0.5% casamino acids. The movements of the fluorescently tagged loci were recorded over a short period of 40 s with 0.1 s intervals (movie s5). Fig. 4a shows a typical image frame with one or two bright loci in each cell. The centroids of the bright dots in each frame were then localized by a custom Matlab program. The trajectory in

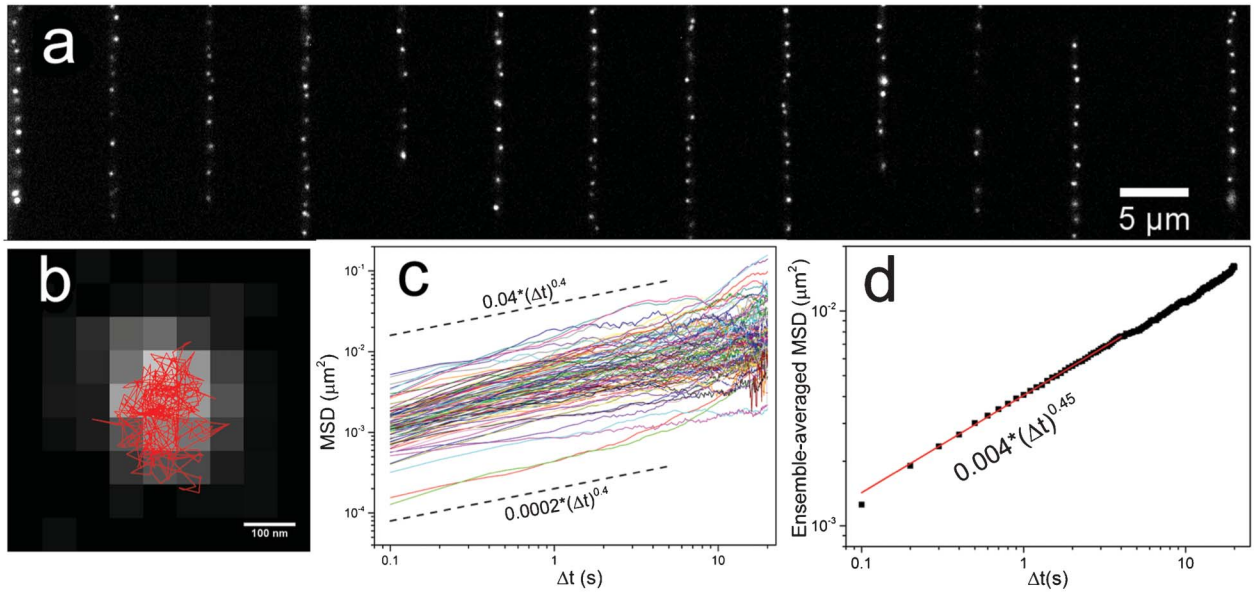

Fig. 4 Movement tracking of chromosomal loci in a typical movie. (a) A fluorescence image frame showing the fluorescently tagged loci (bright dots) inside the *E. coli* cells growing at room temperature (~25 °C) in M9 media supplemented with 0.4% glucose and 0.5% casamino acids and 50 μg mL^{-1} ampicillin. (b) Enlarged view of a single locus and the trajectory (in red) of its centroid over 400 frames. (c) Mean square displacements (MSD) as a function of time interval for individual trajectories. (d) Ensemble-averaged MSD at different time intervals.

Fig. 4b shows that the locus displacement is quite small during the short acquisition time. We calculated the mean-square displacements (MSD) of individual trajectories in the movie, as well as the ensemble-averaged MSDs, as a function of time intervals at short time scales (0.1 to 5 s) and found that the MSD curves are well fit by a power law, MSD = $\gamma(\Delta t)^{\alpha}$, as shown in Fig. 4c & 4d. The same scaling law is observed for all tracking movies and for all loci at various chromosomal positions. The overall distributions of the exponent α at two different growth conditions are shown in Fig. 5. We found that the exponent α calculated from individual loci (Fig. 5a and 5b) has wide distributions under both growth conditions, while the maxima in these distributions are both close to ~0.4. While the shape of the distribution changes slightly, the exponent α calculated from the ensemble-averaged MSD curves for each movie (Fig. 5c and 5d) seems more universal, with mean value of 0.43 ± 0.05 and 0.45 ± 0.04 for the two growth conditions, respectively. This universal exponent agrees with the results obtained from agar experiments by Weber *et al.* at time scales from 1–100 s,[14] although the present work covers shorter time scales, 0.1–5 s.

Conclusions

The present microfluidic chemostat allows the growth of thousands of bacterial cells in the sub-micron channels for many generations while maintaining constant chemical environment and low bacterial populations with a steady age distribution. We can thus measure the bacterial growth dynamics, such as growth rate, cell sizes and GFP expression, at the single-cell level for a much longer time than on a normal agar-based platform. Compared with the agarose-based microfluidic chemostat,[17] the PDMS-based device is easier to fabricate and operate. The pressure-driven loading process is more controllable than by random loading from a diluted suspension. Although PDMS is less permeable to aqueous solutions than agar or agarose, we could still achieve a uniform nutrient environment in the 20 μm-long growth channels by maintaining a weak flow inside the channel.

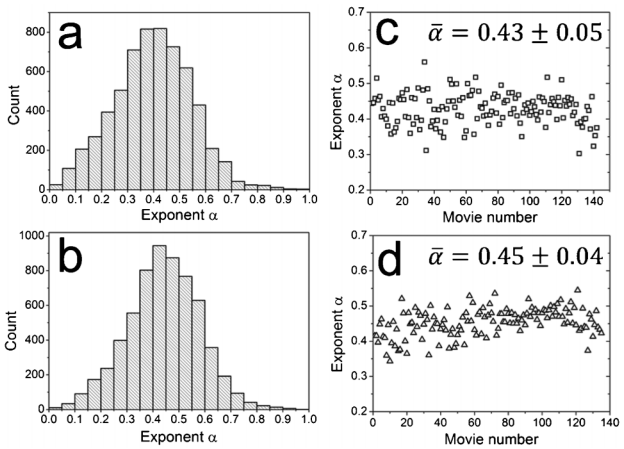

Fig. 5 The distributions of exponent α in different growth media. (a & b) Histograms of α for individual loci in all movies obtained with various strains growing in 'fast' M9 media (a), supplemented with 0.4% glucose and 0.5% casamino acids and 50 μg mL^{-1} ampicillin, or in 'slow' M9 media (b), supplemented with 0.4% glucose and 50 μg mL^{-1} ampicillin. (c & d) Exponent α calculated from ensemble-averaged MSD curves (Fig. 4d) for fast M9 media (c) or slow M9 media (d).

Importantly the present device allows us to quickly change the growth media during the measurements, which extends its uses in many applications that agar-based devices cannot support, such as the addition of specific metabolites to induce gene expression or to test the activity of potential bacterial growth inhibitors. This device can be easily modified to allow for the simultaneous, high throughput measurement of different growth conditions. As we have shown, the liquid growth medium can be uniformly changed to provide a high temporal resolution of the gene expression response and precise control of the growth rate. Biologically, this has high relevance and opens many possibilities, since these transient response regimes (*e.g.* up-shift, down-shift) have been so far characterized with a much lower quantitative detail than balanced growth, particularly at the single-cell level. The open-end channel design also allows us to easily load, grow and immobilize bacterial cells in channels slightly narrower than the cell diameter, making it possible to make time-lapse intracellular measurements with sub-diffraction precision that are infeasible in prior devices that incorporate weak confinement.

We monitored the dynamics of GFP expression in individual *E. coli* cells with a reporter gene construct for over 20 generations in different media. We observed higher expression level in these engineered cells under faster growth rate, as well as different adaptation behaviors after the growth media was changed. We also utilized the microchemostat to track the movement of fluorescently tagged chromosomal loci in *E. coli* cells, finding that the subdiffusive exponent seems to be universally close to 0.4, compatibly with previous findings, independent of the growth rate and the chromosomal positions of loci.

Overall, we were able to obtain data that are similar to those obtained in conventional agar experiments with a significantly more facile and automated platform. We also did not observe any adverse bio-effects from the PDMS environment. We anticipate that the PDMS-based microchemostat presented here will find generic utility in measuring single-cell dynamics in bacteria, in particular at the intracellular level.

Acknowledgements

This work was supported by the HFSP grant RGY0069/2009-C. Portions of this work were performed in the University of Minnesota Nanofabrication Center, which receives partial support from the NSF through the National Nanotechnology Infrastructure Network (NNIN). We thank Anne Olliver for the PgyrA-GFP reporter gene chromosomal construct.

Notes and references

1 M. L. Kovarik, P. C. Gach, D. M. Ornoff, Y. L. Wang, J. Balowski, L. Farrag and N. L. Allbritton, *Anal. Chem.*, 2012, **84**, 516–540.
2 R. N. Zare and S. Kim, *Annu. Rev. Biomed. Eng.*, 2010, **12**, 187–201.
3 D. B. Weibel, W. R. DiLuzio and G. M. Whitesides, *Nat. Rev. Microbiol.*, 2007, **5**, 209–218.
4 G. B. Salieb-Beugelaar, G. Simone, A. Arora, A. Philippi and A. Manz, *Anal. Chem.*, 2010, **82**, 4848–4864.
5 M. R. Bennett and J. Hasty, *Nat. Rev. Genet.*, 2009, **10**, 628–638.
6 J. Nilsson, M. Evander, B. Hammarstrom and T. Laurell, *Anal. Chim. Acta*, 2009, **649**, 141–157.
7 D. Di Carlo, L. Y. Wu and L. P. Lee, *Lab Chip*, 2006, **6**, 1445–1449.
8 A. C. Rowat, J. C. Bird, J. J. Agresti, O. J. Rando and D. A. Weitz, *Proc. Natl. Acad. Sci. U. S. A.*, 2009, **106**, 18149–18154.
9 A. Groisman, C. Lobo, H. J. Cho, J. K. Campbell, Y. S. Dufour, A. M. Stevens and A. Levchenko, *Nat. Methods*, 2005, **2**, 685–689.
10 J. Q. Boedicker, M. E. Vincent and R. F. Ismagilov, *Angew. Chem., Int. Ed.*, 2009, **48**, 5908–5911.
11 J. Park, A. Kerner, M. A. Burns and X. X. N. Lin, *PLoS One*, 2011, **6**, e17019.
12 W. Mather, O. Mondragon-Palomino, T. Danino, J. Hasty and L. S. Tsimring, *Phys. Rev. Lett.*, 2010, **104**, 208101.
13 A. Grunberger, N. Paczia, C. Probst, G. Schendzielorz, L. Eggeling, S. Noack, W. Wiechert and D. Kohlheyer, *Lab Chip*, 2012, **12**, 2060–2068.
14 S. C. Weber, A. J. Spakowitz and J. A. Theriot, *Phys. Rev. Lett.*, 2010, **104**, 238102.
15 Y. Wakamoto, A. Y. Grosberg and E. Kussell, *Evolution*, 2012, **66**, 115–134.
16 P. Wang, L. Robert, J. Pelletier, W. L. Dang, F. Taddei, A. Wright and S. Jun, *Curr. Biol.*, 2010, **20**, 1099–1103.
17 J. R. Moffitt, J. B. Lee and P. Cluzel, *Lab Chip*, 2012, **12**, 1487–1494.
18 P. Lundberg and P. W. Kuchel, *Magn. Reson. Med.*, 1997, **37**, 44–52.
19 A. Pluen, P. A. Netti, R. K. Jain and D. A. Berk, *Biophys. J.*, 1999, **77**, 542–552.
20 J. Ou, M. N. Joswiak, S. J. Carpenter and K. D. Dorfman, *J. Vac. Sci. Technol., A*, 2011, **29**, 011025.
21 C. Saggioro, A. Olliver and B. Sclavi, *Biochem. J.*, 2013, **449**, 333–341.
22 O. Espeli, R. Mercier and F. Boccard, *Mol. Microbiol.*, 2008, **68**, 1418–1427.
23 A. Edelstein, N. Amodaj, K. Hoover, R. Vale and N. Stuurman, *Curr. Protoc. Mol. Biol.*, 2010, 14.20.1–14.20.17.
24 A. E. Carpenter, T. R. Jones, M. R. Lamprecht, C. Clarke, I. H. Kang, O. Friman, D. A. Guertin, J. H. Chang, R. A. Lindquist, J. Moffat, P. Golland and D. M. Sabatini, *Genome Biol.*, 2006, **7**, R100.
25 J. Mannik, R. Driessen, P. Galajda, J. E. Keymer and C. Dekker, *Proc. Natl. Acad. Sci. U. S. A.*, 2009, **106**, 14861–14866.
26 I. Fishov, A. Zaritsky and N. B. Grover, *Mol. Microbiol.*, 1995, **15**, 789–794.
27 M. Z. Liu, T. Durfee, J. E. Cabrera, K. Zhao, D. J. Jin and F. R. Blattner, *J. Biol. Chem.*, 2005, **280**, 15921–15927.
28 S. Klumpp, Z. G. Zhang and T. Hwa, *Cell*, 2009, **139**, 1366–1375.
29 V. G. Benza, B. Bassetti, K. D. Dorfman, V. F. Scolari, K. Bromek, P. Cicuta and M. Cosentino Lagomarsino, *Rep. Prog. Phys.*, 2012, **75**, 076602.

